Processes and Timescales in Onset and Withdrawal of "Aquaplanet Monsoons"

RUTH GEEN, F. HUGO LAMBERT, AND GEOFFREY K. VALLIS

College of Engineering, Mathematics and Physical Sciences, University of Exeter, Exeter, United Kingdom

(Manuscript received 26 July 2018, in final form 22 May 2019)

ABSTRACT

Aquaplanets with low-heat-capacity slab-ocean boundary conditions can exhibit rapid changes in the regime of the overturning circulation over the seasonal cycle, which have been connected to the onset of Earth's monsoons. In spring, as the ITCZ migrates off the equator, it jumps poleward and a sudden transition occurs from an eddy-driven, equinoctial regime with two weak Hadley cells, to a near-angular-momentum-conserving, solstitial regime with a strong, cross-equatorial winter-hemisphere cell. Here, the controls on the transition latitude and rate are explored in idealized moist aquaplanet simulations. It is found that the transition remains rapid relative to the solar forcing when year length and slab-ocean heat capacity are varied, and, at Earth's rotation rate, always occurs when the ITCZ reaches approximately 7°. This transition latitude is, however, found to scale inversely with rotation rate. Interestingly, the transition rate varies nonmonotonically with rotation, with a maximum at Earth's rotation rate, suggesting that Earth may be particularly disposed to a fast monsoon onset. The fast transition relates to feedbacks in both the atmosphere and the slab ocean. In particular, an evaporative feedback between the lower-level branch of the overturning circulation and the surface temperature is identified. This accelerates monsoon onset and slows withdrawal. Last, comparing eddy-permitting and axisymmetric experiments shows that, in contrast with results from dry models, in this fully moist model the presence of eddies slows the migration of the ITCZ between hemispheres.

1. Introduction

The basic features of the onset of Earth's monsoons are seasonal reversal of the wind direction accompanied by intense precipitation. Particularly in the case of the South Asian monsoon, this occurs rapidly relative to the evolution of the solar forcing (Yin 1949; Xie and Saiki 1999). The monsoon systems are localized in longitude, and have often been assumed to be forced by land–sea contrast. However, despite the lack of land–sea contrast, these features of monsoon onset have been identified in aquaplanets with a seasonal cycle and slab-ocean boundary conditions, provided a sufficiently low-heat-capacity ocean is used, for example a 1-m mixed layer depth. Bordoni and Schneider (2008) observed that, in such an aquaplanet model, as the ITCZ shifts off the equator, it undergoes a rapid jump in latitude, coincident with a sudden strengthening of the winter-hemisphere meridional overturning circulation and an enhancement of precipitation. At the surface, in the summer hemisphere, the meridional wind reverses direction from equatorward to poleward, and the zonal wind direction reverses from easterly to westerly. This behavior is associated with a change in the regime of the Hadley circulation from a strongly eddy-driven equinoctial regime, to a near-angular-momentum (AM)-conserving solstitial regime, and is not seen in aquaplanets with deeper mixed layer depths (e.g., 20 m). In these deeper slab-ocean cases, the ITCZ remains near the equator, migrating sinusoidally through the year, and the overturning circulation remains in the equinoctial regime. In simulations where a regime change does occur, the rapidity of the transition relative to the solar forcing suggests that some positive dynamical feedback is involved. In this study, we perform a range of simulations with an idealized moist model to investigate the forcings and feedbacks controlling the rate of aquaplanet monsoon onset, and the ITCZ latitude at which it occurs.

The dynamics of the regime change behavior of the overturning circulation can be understood using the steady-state zonal-mean zonal momentum budget

$$\overline{v}\left(f-\frac{\partial\overline{u}}{\partial y}\right)-\overline{\omega}\frac{\partial\overline{u}}{\partial p}-\frac{\partial\overline{u'v'}}{\partial y}-\frac{\partial\overline{u'\omega'}}{\partial p}+\overline{\mathscr{F}^{(x)}}=0, \quad (1)$$

Corresponding author: Ruth Geen, rg419@exeter.ac.uk

DOI: 10.1175/JAS-D-18-0214.1

where f is the Coriolis parameter; u, v, and ω are the zonal, meridional, and pressure wind speeds; and $\mathscr{F}^{(x)}$ describes frictional damping. Overbars indicate a temporal and zonal mean. Primes indicate deviations from this, corresponding to transient eddies for an aquaplanet. Assuming that streamlines are near horizontal so that vertical derivatives may be neglected, and that friction is weak in the upper troposphere, the leading-order balance in the upper branch of the Hadley circulation is simply

$$\overline{v}(f+\overline{\zeta}) = \frac{\partial \overline{u'v'}}{\partial y}. \tag{2}$$

This equation has two solutions where $\overline{v}$ is nonzero. First, if the eddy term on the right-hand side is zero, then for an overturning circulation to exist, the vertical component of the zonal-mean upper-level relative vorticity, $\overline{\zeta} = -\partial\overline{u}/\partial y$, must balance the planetary vorticity. As $f+\overline{\zeta}$ is proportional to the meridional gradient of AM, this means that the flow must conserve AM. Alternatively, if the eddy term is nonzero, an eddy-driven overturning circulation will exist.

The characteristics of the axisymmetric, AM-conserving regime have been explored extensively, and results from this limit are useful in interpreting the behavior seen in eddy-permitting aquaplanet simulations. Lindzen and Hou (1988) investigated the behavior of the AM-conserving flow for off-equatorial forcings. They showed that for a cell boundary at latitude ϕ_1, at which the zonal wind speed is assumed to be at rest, the AM-conserving zonal wind speed at a latitude ϕ is

$$u = \frac{\Omega a(\cos^2\phi_1 - \cos^2\phi)}{\cos\phi}, \tag{3}$$

where Ω and a are planetary rotation rate and planetary radius, respectively. If the zonal wind is assumed to be in gradient wind balance, by integrating downward a lower-level potential temperature Θ can be evaluated that is associated with the AM-conserving zonal wind (Lindzen and Hou 1988; Schneider and Bordoni 2008):

$$\Theta = \Theta_1 - \Theta_0 \frac{\Omega^2 a^2}{2gH} \frac{(\sin^2\phi - \sin^2\phi_1)^2}{\cos^2\phi}, \tag{4}$$

where g is gravitational acceleration, H is the log-pressure height difference between the lower and upper branches of the Hadley circulation, and Θ_0 and Θ_1 are a reference value and the maximum value of lower-level potential temperature, respectively. For a moist atmosphere, a similar subcloud-layer equivalent potential temperature profile Θ_e in balance with an AM-conserving zonal wind can be formulated (Emanuel 1995; equation amended with missing factor of 2):

$$\Theta_e = \Theta_{e1} \exp\left[-\frac{\Omega^2 a^2}{2c_p(T_s - T_t)} \frac{(\cos^2\phi_1 - \cos^2\phi)^2}{\cos^2\phi}\right]. \tag{5}$$

where T_s and T_t are the temperatures at the surface and tropopause, c_p is the heat capacity at constant pressure, and ϕ_1 is the latitude at which the equivalent potential temperature has its maximum value Θ_{e1}, corresponding to the poleward boundary of the winter-hemisphere Hadley cell. By applying conditions of conservation and continuity of potential temperature at the cell boundaries, Lindzen and Hou (1988) showed that in an axisymmetric model, equatorial heating gives rise to two narrower, weaker Hadley cells, while an off-equatorial heating maximum forces a stronger cross-equatorial cell, with a weaker summer-hemisphere cell. Plumb and Hou (1992) further showed that for an atmosphere relaxing to an equilibrium temperature distribution T_e, with a peak off the equator and a flat gradient elsewhere, some minimum meridional gradient of T_e is needed to force a meridional circulation. They suggested that this threshold behavior might connect to the sudden onset of monsoons.

As seen from (2), eddies allow deviations from these various AM-conserving solutions, so that rather than a weak and narrow equinoctial regime, a stronger eddy-driven equinoctial circulation can be supported (Schneider 1984; Kim and Lee 2001). Schneider and Bordoni (2008) studied the temporal evolution of a circulation of this kind. They found that over the seasonal cycle, the Hadley circulation undergoes rapid regime changes between an eddy-driven, equinoctial state, and an AM-conserving, cross-equatorial state similar to that derived from axisymmetric considerations. To explain the rapidity of the regime change in the aquaplanet model, they proposed a positive feedback process. They found that as the cell moves into the solstitial regime, its lower branch advects cold air up the temperature gradient, pushing the lower-level temperature maximum poleward and steepening the temperature gradient [cf. (4)]. This increase in forcing latitude and temperature gradient results in a stronger overturning circulation (cf. Lindzen and Hou 1988), which in turn strengthens the temperature advection in the lower branch. Additionally, they noted that the upper-level flow in the cross-equatorial Hadley cell is associated with the development of upper-level easterly winds. They suggest that these suppress eddy activity throughout

TABLE 1. Summary of experiments and nomenclature used in text.

Name	Description	X (where relevant)
control	10-m mixed layer depth, 360-day year, Earth's rotation rate	—
opX	As in control, but with the orbital period and mixed layer depth scaled by a factor X	0.25, 0.5, 2, 3, 4
mldX	As in control, but with a mixed layer depth of X m	2.5, 5, 15, 20
no-wishe	As in control, but with dependence of surface heat exchange on the wind speed removed	—
rtX	Based on control, mld5 and mld15, but with the rotation rate scaled by a factor X	0.5, 0.75, 1.25, 1.5, 1.75, 2
control-zs	Axisymmetric simulation with SSTs prescribed to those of control	—

the tropics, helping to transfer the circulation to the AM-conserving regime. The AM-conserving cell is intensified by the lower-level thermal forcing, resulting in stronger easterlies and a positive feedback. In a later study, they demonstrated that a similar regime change is also observed in a seasonally evolving dry axisymmetric model, but found that eddies appear to sharpen the transition (Bordoni and Schneider 2010).

A range of studies have now identified changes in the regime of the zonal momentum budget during the onset of Earth's monsoons (Shaw 2014; Walker and Bordoni 2016; Geen et al. 2018). It therefore seems useful to return to the relatively simple aquaplanet case and determine the controls on the ITCZ latitude at which the regime change occurs, and the rate of the transition. By exploring these using an idealized moist model, we hope to determine which basic factors, besides land–sea contrast, control the onset of the real-world monsoons. To approach this, we use a range of simulations to explore the effects of year length, slab-ocean mixed layer depth, planetary rotation rate, wind-induced surface heat exchange (WISHE), and eddies. In what follows, "equinoctial regime" refers to a circulation where the ITCZ is on or close to the equator, so that two Hadley cells of approximately similar strength exist. Where eddies are permitted, this state is eddy-driven. "Solstitial" regime refers to the circulation where the ITCZ is far from the equator and the overturning circulation is cross-equatorial and close to AM-conserving. The remainder of the paper is structured as follows: section 2 describes the model used and details of the simulations performed. Results are presented in sections 3–6. Section 7 concludes the paper.

2. Model and experiments

We use the idealized modeling framework Isca, which is described in full in Vallis et al. (2018). This is based around the GFDL spectral dynamical core, and has a range of parameterizations allowing the atmospheres of both Earth and other planets to be simulated. Here, as in Geen et al. (2018), we use a setup similar to the Model of an Idealized Moist Atmosphere (Jucker and Gerber 2017). This includes simple parameterizations of moist physics based on the idealized model of Frierson et al. (2006). The convection scheme is the simplified Betts–Miller scheme described in Frierson (2007), with the amendments of O'Gorman and Schneider (2008). Experiments are run at T42 resolution, on 40 unevenly spaced sigma levels, and with a 720-s time step. A key difference from the Frierson et al. (2006) physics is the inclusion of a more comprehensive radiation scheme, the Rapid Radiative Transfer Model (RRTM; Mlawer et al. 1997; Clough et al. 2005). This recalculates radiative heating, based on the humidity and temperature structure of the atmosphere, every 3600 s of model time. The insolation includes a seasonal and diurnal cycle, with a circular orbit, a solar constant of 1360 W m^{-2}, and an Earth-like obliquity of 23.439°. As is common in idealized models, clouds are not included in the parameterization of moist processes or of radiation. At the surface, a slab ocean allows for a closed atmospheric energy budget. The temperature of the slab is controlled by the radiative, sensible, and latent heat fluxes at the sea surface following

$$C\frac{\partial T_s}{\partial t} = R_S + R_L + H_L + H_S, \tag{6}$$

where C is the surface heat capacity; T_s is the sea surface temperature (SST); R_S and R_L are the net downward shortwave and longwave fluxes at the surface, respectively; H_L is the latent heat flux; and H_S is the sensible heat flux. As in Geen et al. (2018), a surface albedo of 0.25 is prescribed, with a high value chosen to compensate for the lack of clouds in the model. At the top of the model, a sponge layer is applied to inhibit gravity wave–like behavior.

The experiments performed are summarized in Table 1, which additionally provides a reference for the nomenclature used to identify them. A control simulation is used as a baseline for comparison with the other experiments. This has an Earth-like rotation rate and orbital period, and a 10-m mixed layer depth. The control uses a 30 day month^{-1} calendar, so that a control year is 360 days.

Section 3 discusses the results of experiments in which the orbital period and mixed layer depth are varied. In the opX experiments, the orbital period, and consequently year length, of the planet is altered by a factor $X = P/P_E$ where P is the amended period, and P_E is the period of Earth's orbit. To keep the magnitude and structure of the seasonal cycle of surface temperatures similar between the various opX experiments, the control mixed layer depth is also multiplied by this factor, so that for example the op2 experiment has a mixed layer depth of 20 m. The mldX experiments have a mixed layer depth of Xm, but Earth's orbital period.

In section 4, to investigate the role of WISHE, the control experiment is compared with an experiment denoted no-wishe, in which the wind speed used in calculating the surface evaporation and sensible heat transfer is prescribed to $10\,\mathrm{m\,s^{-1}}$ at all grid points. This value is chosen based on the global-mean lowest-level wind speed of the control run. This simulation also gives some indication of the role of moisture–radiation interactions as a source of feedbacks, as without this interaction with the wind speed, surface cooling is predominantly controlled by the surface and lowest-model-level temperatures, and the radiative fluxes.

In section 5 we present results from the rtX experiments, where the planet's rotation rate is varied by a factor $X = \Omega/\Omega_E$, where Ω_E is Earth's rotation rate. To confirm that results from these experiments are robust under changes to other parameters, simulations are repeated for all rotation rates using mixed layer depths of 5 and 15 m.

Last, in section 6, the role of eddies is explored by comparison of the control with an experiment control-zs, which is an axisymmetric simulation forced with the SSTs of the control experiment. In this experiment, similar to previous studies in axisymmetric models (e.g., Satoh 1994; Caballero et al. 2008), vertical diffusion is enabled in the free atmosphere to suppress symmetric instabilities, though some noise is still evident.

All experiments were spun up for 3600 days (10 years in control simulation time), except for the op3 and op4 experiments, which were spun up for 4320 days to allow averages to begin in the experiments' Januarys. Seasonal climatologies were then averaged over 30 experiment years, corresponding to 10 800 days in experiments with control length years, or e.g., 5400 and 21 600 days for op0.5 and op2, respectively. The data presented comprise climatologies of multiyear 5-day (pentad) means, except for experiment op0.25 where the very short year length means that this would give only 18 data points, and multiyear daily means are instead presented. For all runs, the climatologies are hemispherically averaged, so that, for example, Northern Hemisphere January is averaged with Southern Hemisphere June. Confidence intervals on the transition rates and latitudes identified in the simulations are evaluated using a bootstrapping technique (e.g., Wilks 2011, 172–174).

3. Forcing and response time

The seasonal migration of the ITCZ is forced by the change in insolation over the year, and consequent variation of the interhemispheric temperature gradient (Bordoni and Schneider 2008). As a lowest-order approach to understanding the seasonal shifts of the ITCZ, we therefore investigate the response of the model when we vary the orbital period of the aquaplanet such as to slow down or speed up the rate of the seasonal cycle.

To identify the ITCZ location in our simulations, we evaluate the precipitation centroid, which we define as the latitude that is the centroid of the area-integrated precipitation from 45°S to 45°N. Although previous studies have defined this purely over tropical latitudes (Frierson and Hwang 2012; Donohoe et al. 2013), due to the variety of climates explored in our simulations we use a larger range of latitudes. We find that this gives a reasonable estimate of ITCZ latitude and does not appear biased by midlatitude precipitation in all experiments, with the exception of the no-wishe simulation, for which it is therefore not used.

Figure 1a shows the seasonal cycle of the precipitation for the control run. Also shown is a 500-hPa cross section of the meridional overturning streamfunction,

$$\Psi = \frac{2\pi a}{g}\cos\phi\int_0^{p_s}[\bar{v}]\,dp\,, \tag{7}$$

where p_s is surface pressure (see Fig. 8 for examples of the latitude–pressure structure). The black line indicates the precipitation centroid. Looking at Northern Hemisphere spring and summer, the two regimes described in section 1 can be seen from the strength of the precipitation and overturning circulation. From pentad 28 to 44, the precipitation is centered near the equator in a narrower band, and two Hadley cells of comparable strength exist. Between pentads 44 and 48 the precipitation centroid moves rapidly north, before slowing again after reaching approximately 15°N. In this time, the circulation has shifted to the solstitial regime, with a strong cross-equatorial winter cell and weak summer cell, and more intense precipitation. This regime persists for approximately 2 months (12 pentads). The precipitation centroid then migrates more

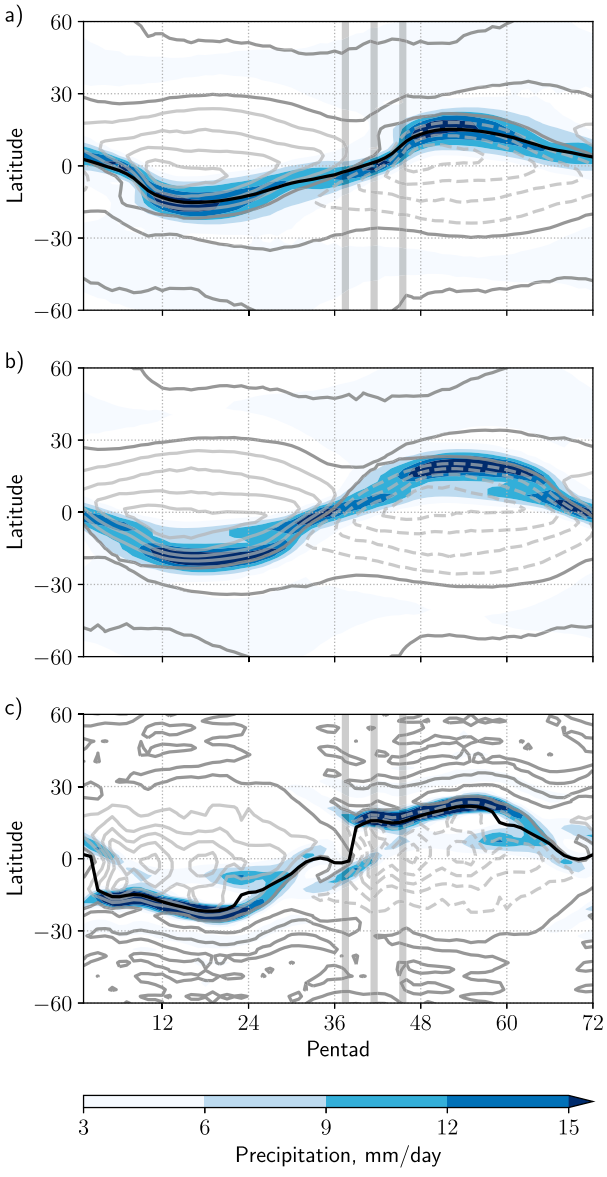

FIG. 1. Seasonal cycle of precipitation (colors) and 500-hPa "slice" of the meridional overturning circulation (gray contours, interval: 100×10^9 kg s^{-1}) for the (a) control, (b) no-wishe, and (c) control-zs experiments. Where shown, the precipitation centroid is indicated by the black line, and the zero overturning line is shown in dark gray. Dashed gray contours indicate negative values of the meridional overturning circulation. Note that pressure–latitude plots of the overturning in control and control-zs are shown in Fig. 8, which are time averages taken over the gray-shaded bars from this figure.

gradually back toward the equator, and the equinoctial regime is reestablished.

It might be expected intuitively that the ITCZ would migrate sinusoidally following the subsolar point; but insolation is predominantly communicated to the atmosphere via the SST, and atmospheric circulations are driven by gradients of temperature. These may not evolve smoothly like the subsolar point. However, a simple linearized model of the interhemispheric contrast in near-surface air temperature indicates that, neglecting changes in the regime of the overturning circulation throughout the year, the thermal gradient is indeed expected to evolve sinusoidally (Zhou and Xie 2018). Seasonal changes in the circulation regime (cf. Bordoni and Schneider 2008) induce deviations from this estimate, and it can be seen that the precipitation centroid in Fig. 1a does not follow a sinusoidal path throughout the year.

Deviations from a sinusoid can be diagnosed by plotting the rate of movement of the precipitation centroid against its latitude. In this space, a simple harmonic oscillator, with a sinusoidal change in displacement with time, would be expected to follow an ellipse. The trajectory for the control simulation is shown by the black line in Fig. 2a, and is clearly not sinusoidal. At low latitudes, the migration rate is small, approximately 0.2° day^{-1}. During the shift of the precipitation centroid off the equator, the rate increases, peaking at 0.5° day^{-1} at 7.7°. The rate then slows and the precipitation centroid moves more gradually out to its maximum latitude of roughly 15°, before the direction of movement changes and the precipitation centroid returns slowly toward the equator.

Figure 2a also shows the trajectories for the opX simulations. In op0.25, ITCZ migrations are small. No regime change occurs, and the trajectory follows an ellipse, consistent with solar forcing being the sole driver in this case. Allowing for the change in the seasonal cycle length, other simulations show similar behavior to the control, including a peak in the rate of movement as the precipitation centroid shifts off the equator. As the model has more time to equilibrate, the maximum latitude that the ITCZ reaches increases with length of year, beginning to level out in the longest-year-length runs (red circles, Fig. 2c). Despite this increase in maximum latitude with year length, the peak rate of migration of the ITCZ remains at a similar latitude in all simulations where a regime change occurs (black circles, Fig. 2c), with an average of 7.1° ± 1.2° (uncertainty interval corresponds to two standard deviations). This indicates that the latitude at which the transition occurs is independent of the length of the year.

The rate of ITCZ migration also varies between simulations. The black and red circles in Fig. 2b show the dependence on orbital period of the peak rate of movement of the ITCZ and the rate of change of the ITCZ's latitude as it crosses the equator, respectively.

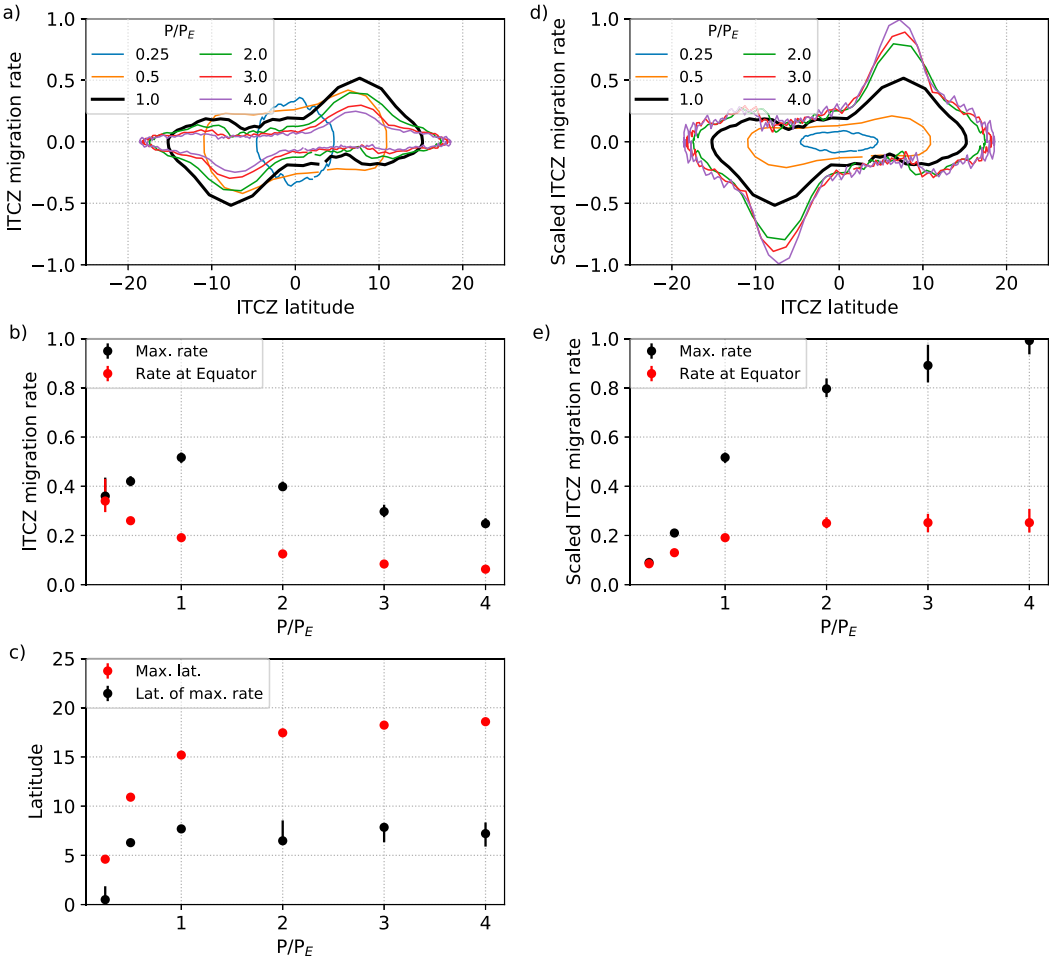

FIG. 2. (a) Latitude of the precipitation centroid (°) vs rate of movement of the precipitation centroid (° day^{-1}) for the opX experiments, in which the aquaplanet's orbital period and mixed layer depth are multiplied by a factor $X = P/P_E$ (see Table 1). The control experiment is indicated by the heavy black line. (b) ITCZ migration rate as a function of P/P_E. Black circles indicate the maximum rate for each run, and red circles indicate the rate at the equator. (c) Maximum latitude the ITCZ reaches (red circles) and latitude at which the peak rate of ITCZ migration occurs (black circles). (d),(e) As in (a) and (b), respectively, but with the rate of movement of the precipitation centroid now also scaled by X. Lines in (b), (c), and (e) indicate the 95% confidence interval evaluated using a bootstrapping technique.

The peak migration rate increases with season length up to the control, then decreases as the planet's orbit rate slows further. The rate of movement as the ITCZ crosses the equator is used as an indicator for the rate of ITCZ migration at other times of year than during the regime change, and is seen to decrease as the orbital period is slowed.

To assess over which sections of the annual cycle the rate of movement of the ITCZ scales with the rate of change of the insolation, Figs. 2d and 2e show equivalent plots to Figs. 2a and 2b, but with the ITCZ migration rate scaled by P/P_E. Aside from during the regime transition, the trajectories for the three slowest orbiting experiments overlap throughout the year, and the red circles in Fig. 2e now level out at a value of 0.25° day^{-1}. This shows that for a sufficiently long year length, in both the equinoctial and solstitial regimes, the rate of ITCZ migration is directly proportional to the rate of change of the solar forcing. In contrast, the peak rates, which occur over monsoon onset, do not scale proportionately to the orbital period, with the scaled peak rates continuing to increase with year length. Over onset, the ITCZ migration rate is therefore not purely forced by insolation, and is fast relative to this, indicating that a positive feedback occurs once the ITCZ moves some distance from the equator. We note that the difference in behavior for the shorter year lengths indicates that scaling the mixed layer depth

does not perfectly compensate for the longer year length, but the convergence of the trajectories as year length increases suggests this is still a reasonable approach to produce comparable experiments.

The results from the mldX experiments, shown in Fig. 3a, allow exploration of the role of the response time of the surface and of the behavior in configurations where the maximum ITCZ latitude and the temperature gradient will vary widely. For a deep mixed layer depth, as in mld20, the ITCZ remains close to the equator throughout the year, and the experiment remains in the equinoctial regime. The maximum latitude reached increases as mixed layer depth decreases, and in mld5 and mld2.5 the ITCZ moves farther poleward than was seen in the opX experiments. We find that the maximum latitude scales linearly with mixed layer depth (see Fig. 3c), and may be fitted with a relation:

$$\phi_{\max} = 25.9 \pm 1.7 - (0.99 \pm 0.14) X_M, \qquad (8)$$

where X_M is the mixed layer depth as indicated in the mldX experiment names. The intercept of the above equation implies that for a zero or infinitesimally small mixed layer depth, or at perpetual solstice, the amplitude of the ITCZ migration has a maximum of 26° (at Earth's obliquity). This is consistent with previous research into the ITCZ latitude in perpetual solstice simulations (e.g., Faulk et al. 2017).

We also see that as mixed layer depth decreases, the rate of movement of the ITCZ increases both in the equinoctial regime and during the regime change, showing that the surface is responding to the insolation more quickly. The rate on the equator and the peak rate are again plotted in Fig. 3b. We find that these may be fitted with relations

$$R_{\text{eq}} = 0.08 \pm 0.02 + \frac{0.96 \pm 0.10}{X_M} \qquad (9)$$

and

$$R_{\max} = 0.89 \pm 0.07 - (0.039 \pm 0.006) X_M, \qquad (10)$$

respectively. It appears that the maximum latitude reached is proportional to the maximum migration rate, and that this is limited by the mixed layer depth. The difference between the relationships of the migration rate at the equator and the peak rate is interesting. The inverse scaling on the equator suggests that, aside from during the Hadley cell regime change, the model has a response time proportional to the mixed layer depth. However, over the regime change, feedbacks result in a linear relationship between the peak rate and mixed layer depth. Note that, in the limit

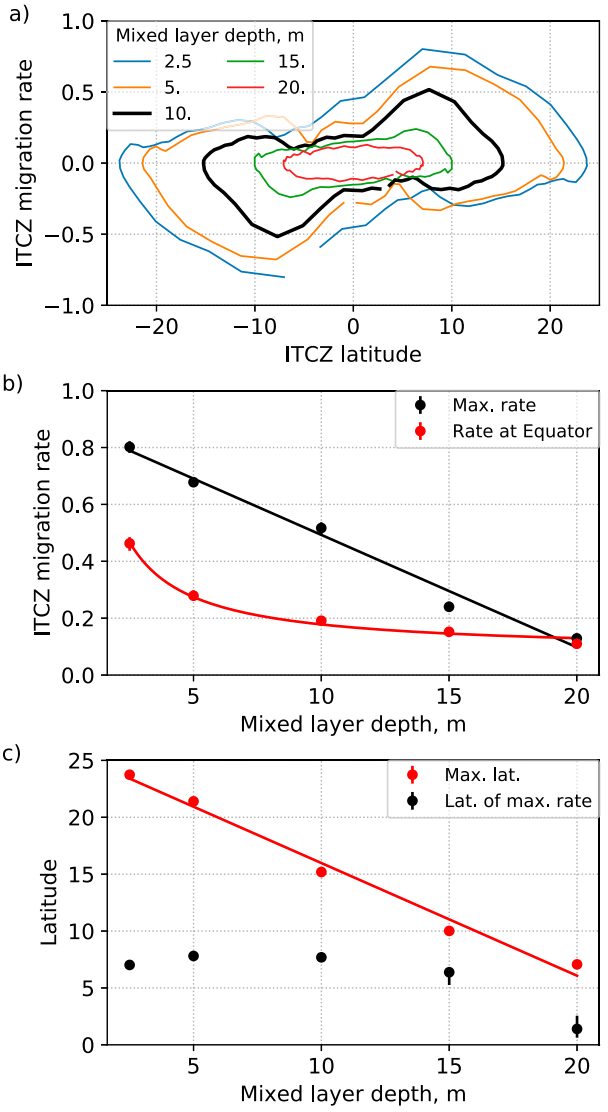

FIG. 3. As Figs. 2a–c, but for the runs in which mixed layer depth (but not orbital period) is varied. Lines are fits to the data following (8)–(10).

of a large mixed layer depth, for example, the 20-m simulation shown in Fig. 3a, there is no regime change, and we anticipate that the peak ITCZ migration rate will follow (9).

Last, we also note that, as in the opX experiments, the latitude at which the peak rate occurs is similar in all of the mldX experiments where a regime transition occurs, this time with an average of 7.2° ± 1.2°. This latitude is consistent with that from the opX experiments, and shows little variation with mixed layer depth despite the wide range of maximum latitudes reached by the ITCZ. This consistency suggests that the feedbacks governing the regime change have some dependence on latitude. Having demonstrated in this section that

the transition rate and latitude are not simply governed by the rate of forcing, in the remainder of the paper we explore the controls on these features of the seasonal cycle.

4. Temperature feedbacks

One potential process that could cause a fast transition from the equinoctial to solstitial regime is a positive feedback between the cell strength and the location of the maximum in lower-level moist static energy, which is known to be correlated with the ITCZ latitude (Privé and Plumb 2007). As discussed in section 1, Schneider and Bordoni (2008) identified such a feedback between the cell strength and the 850-hPa meridional temperature gradient. In our moist simulations we observe behavior consistent with this. In contrast with Schneider and Bordoni (2008), who relax the SSTs to a prescribed profile, our simulations also include a slab ocean whose temperature interacts with the atmosphere, providing an additional possible source of feedbacks through seasonal modifications of the SST, for example via WISHE. In axisymmetric models, WISHE has been shown to be able to cause a transition to a cross-equatorial AM-conserving flow in circumstances where forcing is weak and this would not otherwise occur, and, for stronger forcings, to shift the transition earlier in the seasonal cycle (e.g., Boos and Emanuel 2008a,b). To explore the role of WISHE in the transition in our simulations, we compare the control with the no-wishe experiment, in which the surface latent and sensible heat fluxes do not depend on the lowest model level wind speed.

Figures 1a and 1b show the zonal-mean precipitation as a function of time and latitude for the control and no-wishe experiments. Similarly to the control simulation, the peak precipitation in no-wishe does not migrate sinusoidally, consistent with the temperature advection feedbacks of Schneider and Bordoni (2008). In fact, we now find that there is not only a jump in the location of the ITCZ during the transition from the equinoctial to the solstitial regime, but also during the reverse transition. As this is not seen in the control, where the surface heat fluxes respond to the atmospheric wind speed, we deduce that WISHE slows the return of the ITCZ to the equator here.

To identify the cause of this difference, we look at the evolution of the SSTs throughout the year in the simulations. Figure 4a shows the climatological SST for the control experiment. Similarly to the precipitation centroid (Fig. 1a), it can be seen that the peak SST does not migrate sinusoidally. While the ITCZ is near the equator, warm SSTs expand over latitudes between the equator and 25° in the "spring" hemisphere. Additionally, temperatures below the ITCZ remain warm in the "autumn" hemisphere during the ITCZ's return toward the equator. This behavior is not seen in the no-wishe experiment, shown in Fig. 5a, where the temperature structure is more symmetric between monsoon onset and withdrawal, consistent with the behavior of the precipitation in this experiment.

To investigate how the SSTs are influenced by WISHE, in Figs. 4b and 5b we plot the rate of change of the SST, and in Figs. 4c–f and 5c–f the surface energy fluxes whose imbalance drives the SST change [right-hand side of (6)]. The rate of change of SST is dominantly controlled by the pattern of shortwave heating, with the longwave and latent heat fluxes acting to cool the surface and prevent an increase in the global annual-mean temperature. Under the Hadley cells, where the air contains more moisture, the net upward longwave heat flux is weaker in magnitude. The moist air reemits more radiation downward back toward the surface, reducing the surface cooling here. In this region, the latent heat flux is instead the dominant cooling mechanism for the surface.

Figures 4f and 5f suggest that the latent heat flux is responsible for the slower decrease in SST as the ITCZ returns toward the equator. During this phase of the seasonal cycle, in the control a minimum in evaporative cooling can be seen beneath the ITCZ. This minimum in evaporative cooling is not present in the no-wishe experiment. To identify the cause of this minimum, in Fig. 6 we divide the evaporative cooling in the control into its constituent parts, using

$$H_L = L\rho_a C_d |\mathbf{v}_a| (q_a - q_s). \tag{11}$$

In (11), ρ_a, $|\mathbf{v}_a|$, and q_a are the density, horizontal wind speed, and specific humidity at the lowest model level, respectively; L is the latent heat of vaporization of water; C_d is the drag coefficient; and q_s is the saturation specific humidity at the surface temperature [cf. Eq. (11); Frierson et al. 2006].

Figure 6a shows the difference in the specific humidity of the lowest model layer and the saturation specific humidity at the surface temperature. This has its largest magnitude below the ITCZ throughout the year, and hence cannot explain the minimum in evaporative cooling. The air density (Fig. 6b) is predominantly controlled by temperature, and so is lowest near the equator, increasing toward the poles. This does not exhibit any finer structure resembling Fig. 4f. However, we see that the lower-level wind speed magnitude (Fig. 6c) has a minimum value below the ITCZ when this is near the equator, before increasing as the cell shifts to the cross-equatorial,

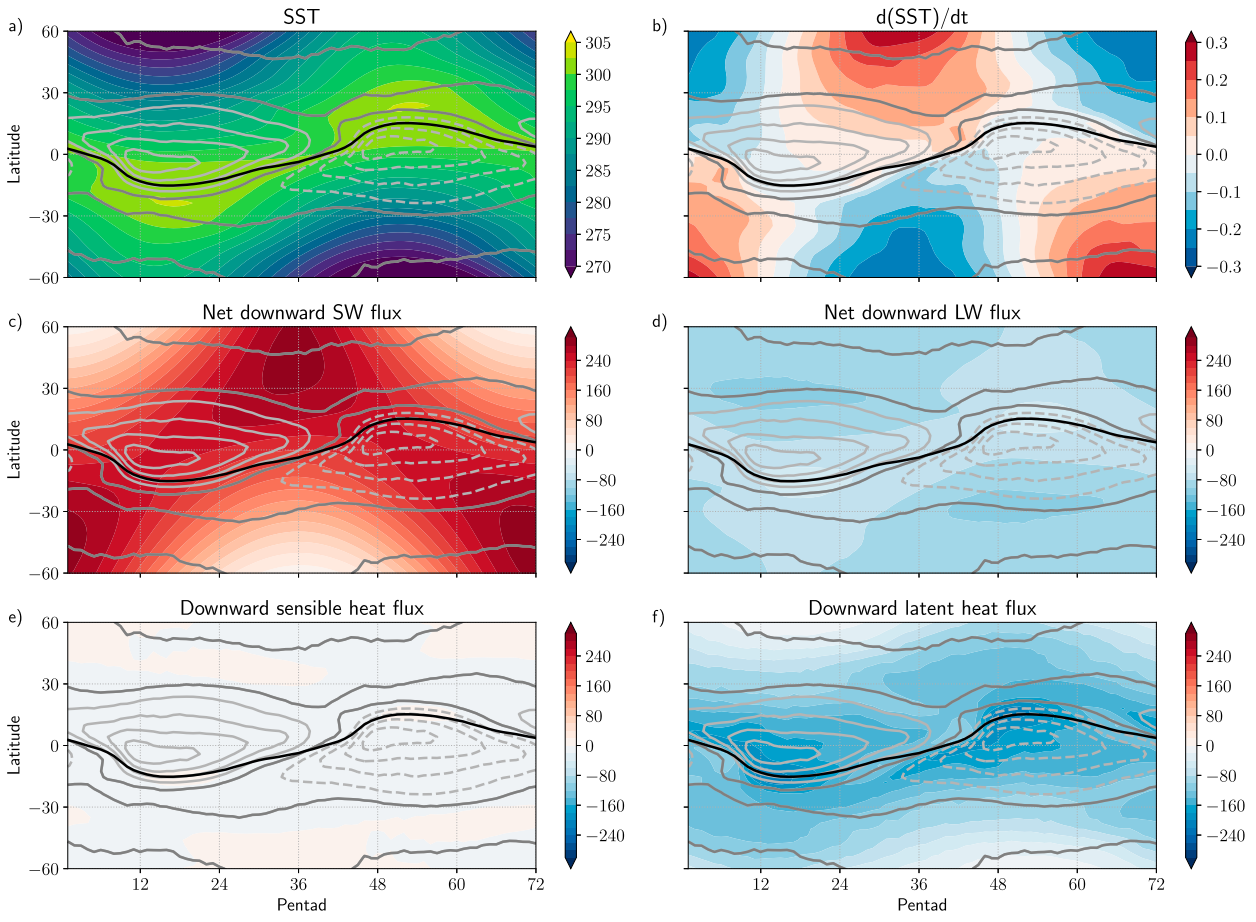

FIG. 4. Seasonal cycle of (a) SST (K), (b) the rate of change of SST (K day^{-1}), and the net surface fluxes (W m^{-2}), directed downward, of (c) shortwave and (d) longwave radiation, (e) sensible heat, and (f) latent heat in the control. The precipitation centroid and 500-hPa overturning circulation are shown for reference, as in Fig. 1.

solstitial regime. We conclude that the minimum in evaporative cooling is due to the low horizontal wind speeds below the narrow ascending region in the equinoctial regime. The reduced cooling causes the SST to remain warmer for longer, slowing the return of the ITCZ to the equator. In Fig. 1, it can also be seen that the zero line of the meridional streamfunction jumps off the equator at the start of summer in the control experiment, while it migrates more smoothly in the no-wishe experiment. This suggests that, in addition to slowing withdrawal, the reduced evaporative cooling also acts to accelerate monsoon onset. Once the ITCZ crosses the equator, the reduced cooling beneath it helps to warm the summer hemisphere, encouraging the transition to the solstitial regime.

An additional possible source of asymmetry between onset and withdrawal is moisture–radiation interactions within the atmospheric column, for example, via enhanced absorption or emission of radiation due to the column moisture content, which could modify the SST or lower-level temperatures. In the no-wishe experiment, the SST depends only on the incident insolation and the contrasts in temperature and humidity between the surface and lowest model level, rather than on lowest-level wind speed. In addition to helping to separate out the role of WISHE, the no-wishe experiment therefore also gives some insight into the importance of these moisture–radiation interactions. Figure 5c shows the net shortwave flux at the surface in colors, and the insolation in gray contours. It can be seen that absorption of shortwave radiation by water vapor results in a slight change in the seasonally evolving structure of the surface flux from that of the incident flux. For example, the subsolar point migrates into the Northern Hemisphere at roughly pentad 16. As the Northern Hemisphere is cooler at this time, it contains less water vapor. Shortwave absorption is relatively weak. As the Northern Hemisphere begins to warm, more water vapor is in columns at a given latitude, resulting

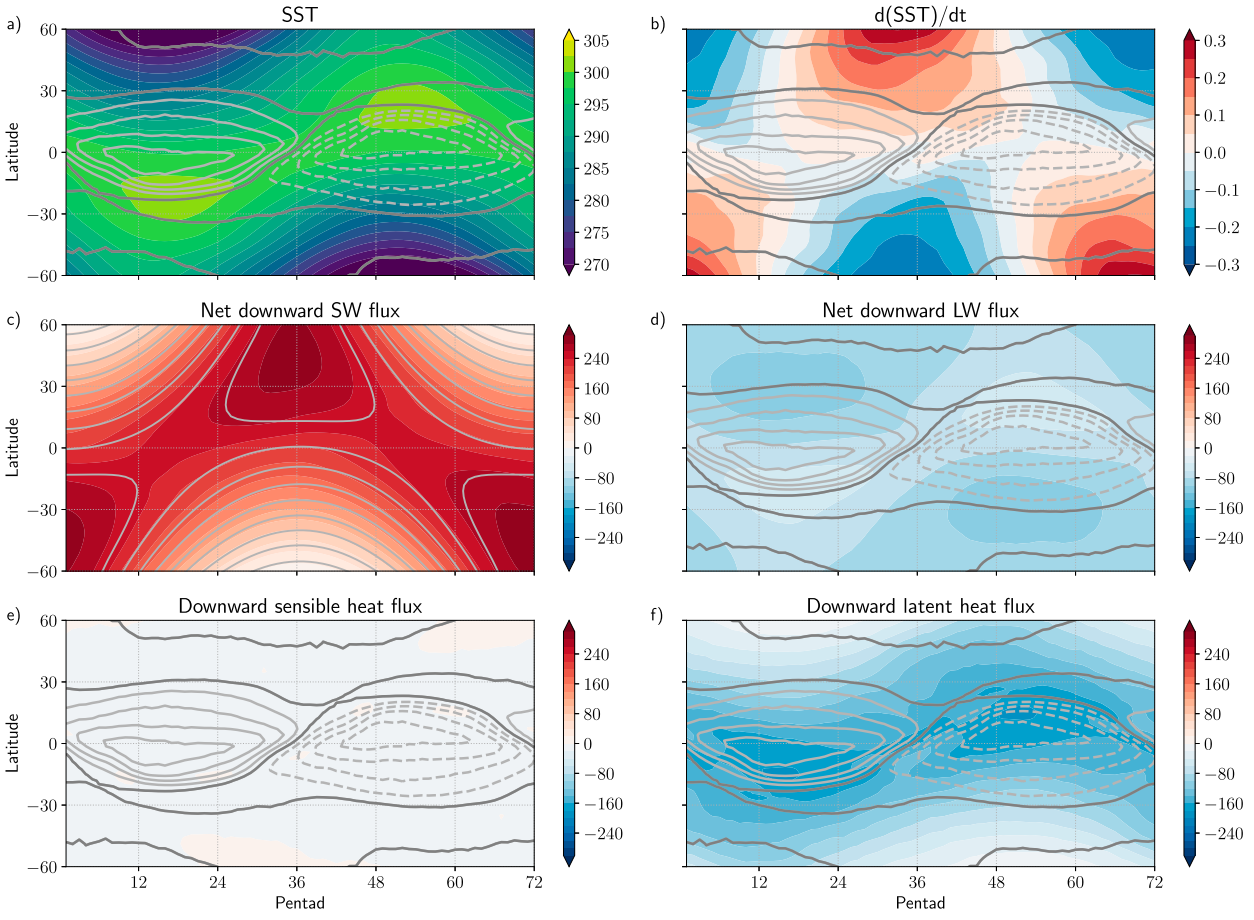

FIG. 5. As in Fig. 4, but for the no-wishe experiment. Note that here the precipitation centroid is not shown, as this was found to give a poor estimate of the ITCZ location for this experiment. Also, in (c), the insolation is shown with gray contours, with a contour interval of 50 W m^{-2} (maximum contour is 450 W m^{-2}).

in more absorption and a slight decrease in magnitude of the shortwave surface flux. However, compared with the WISHE feedbacks, this moisture–radiation effect appears small, as for example, the warming and cooling of each hemisphere in the no-wishe experiment SST is almost symmetric compared with the control (see Figs. 4a and 5a).

Although the differences between the control and no-wishe experiments show that interactions between the surface and atmosphere do modulate aquaplanet monsoon onset and withdrawal, that rapid transitions are observed in no-wishe shows that processes internal to the atmosphere are likely more important. The remainder of the paper will explore these internal feedbacks in more detail. We additionally note that the presence of clouds would significantly alter the shortwave and longwave fluxes, and that a coupled ocean might strongly alter the balance of surface fluxes. We hope to explore these factors in future work.

5. Effect of varying the rotation rate

In section 3, it was observed that the transition latitude does not vary when mixed layer depth is varied, despite the resulting changes to, for example, the meridional temperature gradient and the maximum latitude reached by the ITCZ. From (3) and (5), it can be seen that altering planetary rotation rate or radius will alter the AM-conserving zonal wind and equivalent potential temperature profiles. In this section, we therefore investigate whether varying planetary rotation rate alters the transition latitude, as changing mixed layer depth and orbital period did not.

Figures 7a–c show the latitude and rate of movement of the precipitation centroid for the rtX simulations for mixed layer depths of 5 (top), 10 (center), and 15 m (bottom). The same basic features as in the control experiment are again seen, with a peak in migration rate once the ITCZ moves sufficiently far from the equator, so that the trajectory deviates from the ellipse

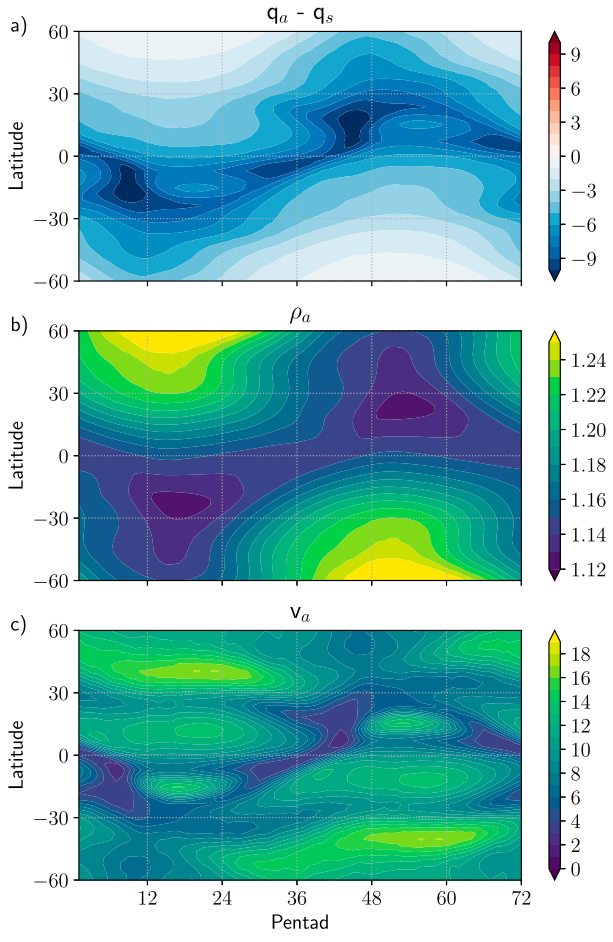

FIG. 6. Terms contributing to the modeled surface flux of latent heat. (a) Difference between lowest-model-layer specific humidity and saturation specific humidity at the surface temperature ($g\,kg^{-1}$). (b) Air density at the lowest model level ($kg\,m^{-3}$). (c) Absolute horizontal wind speed at the lowest model level ($m\,s^{-1}$).

that would be expected for simple harmonic oscillator-like behavior. As rotation rate decreases, the ITCZ reaches progressively higher latitudes, consistent with theories for the solstitial Hadley cell (Lindzen and Hou 1988; Caballero et al. 2008). In contrast to the results of the mldX simulations, where transition latitude remained similar in all experiments, here we find that the transition latitude decreases with increasing rotation rate, as shown in Fig. 7e.

This change in the transition latitude in the rtX experiments might be interpreted in relation to changes of the equivalent potential temperature gradient associated with the AM-conserving wind as planetary rotation changes, and in how the momentum and vorticity budgets rebalance during the regime change. Looking at (5), we find that this equivalent potential temperature gradient decreases as rotation rate decreases, but increases as ϕ_1 increases. We might therefore interpret the behavior seen in Fig. 7e as a need for ITCZ latitude to increase as rotation rate decreases in order to produce the same equivalent potential temperature gradient, and consequently similar thermal forcing and feedbacks on the meridional circulation, as discussed in section 1. However, relating this to the observed change in latitude is challenging, as it is not clear at which latitude the equivalent potential temperature gradient should be considered, and further, the theoretical equivalent potential temperature gradient does not consistently match the modeled profiles as rotation is varied (not shown). Alternatively, Geen et al. (2018) noted a sudden increase in magnitude of the vortex stretching term in the vorticity budget during the regime change, so that, over the ITCZ, during onset this became the dominant term in the budget, that is,

$$\frac{\partial \overline{\zeta}}{\partial t} \sim -(f+\overline{\zeta})\nabla \cdot \overline{u}. \tag{12}$$

A reduction in $\overline{\zeta}$, so that $f+\overline{\zeta}$ approaches zero, would result in an upper-level flow nearer to an AM-conserving state; see (2). If this process mediates monsoon onset, the increase in the transition latitude as rotation rate is decreased might alternatively be interpreted as the ITCZ needing to travel further from the equator when rotation rate is decreased in order for vortex stretching to become significant. However, we find in our simulations that the ITCZ begins to move rapidly prior to the increase in this term and to the decrease in upper-level absolute vorticity. With neither approach appearing to explain the observed behavior, we leave a complete explanation of this for future work.

While the transition latitude decreases monotonically with rotation rate, Fig. 7d shows that the transition rate does not follow such simple behavior. Interestingly, this instead has a maximum at Earth's rotation rate, possibly implying that the rotation rate of Earth is such as to make the planet particularly susceptible to a rapid onset of monsoon precipitation. The results of the simulations with 5- and 15-m mixed layer depths, shown by red and blue circles, respectively, confirm that the maximum rate is still at Earth's rotation rate when the response time of the model is altered.

Analysis of the Rossby number and decomposition of the overturning circulation into mean-flow and eddy-driven components (cf. Schneider and Bordoni 2008) for the slow-rotation-rate experiments (not shown) confirms that these do enter an eddy-driven regime while the ITCZ is near the equator. This indicates that the slower peak ITCZ migration rates in these cases are not due to a lack of a regime change. We suggest that the slow transition rates at low rotation rate might relate

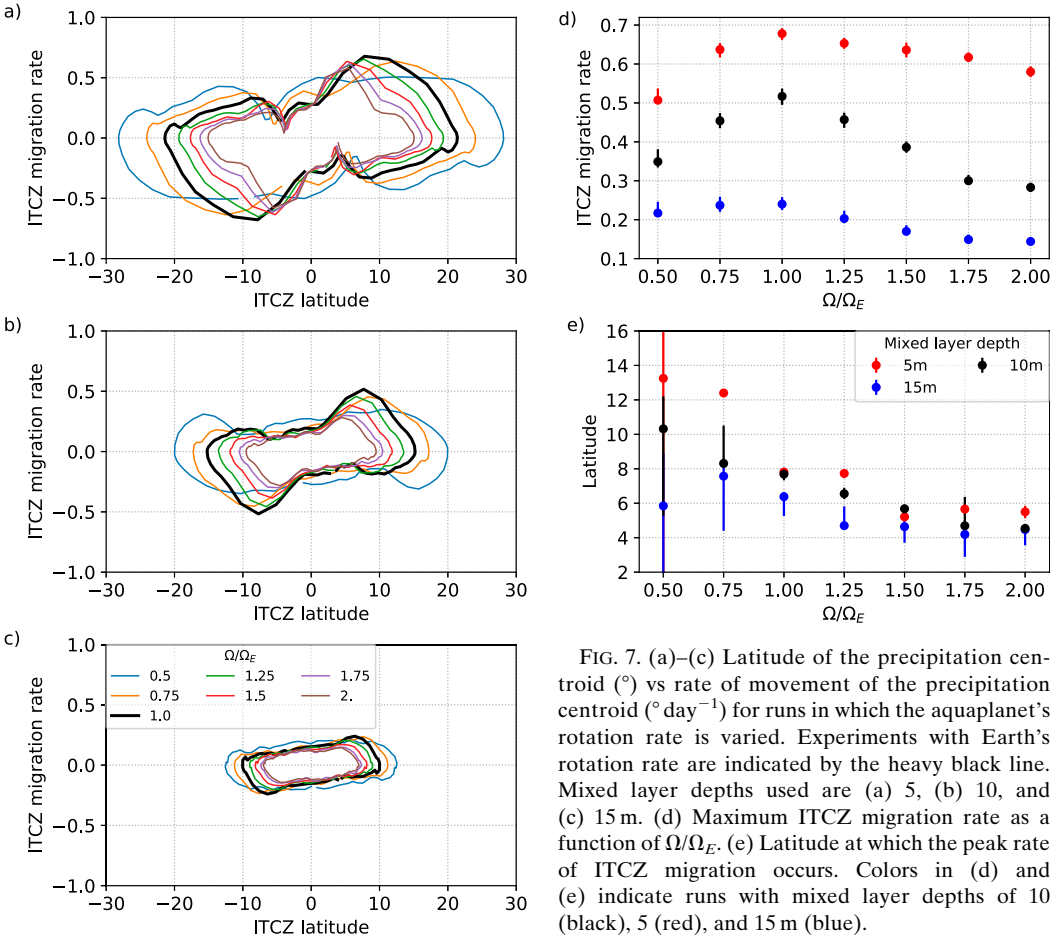

FIG. 7. (a)–(c) Latitude of the precipitation centroid (°) vs rate of movement of the precipitation centroid (° day^{-1}) for runs in which the aquaplanet's rotation rate is varied. Experiments with Earth's rotation rate are indicated by the heavy black line. Mixed layer depths used are (a) 5, (b) 10, and (c) 15 m. (d) Maximum ITCZ migration rate as a function of Ω/Ω_E. (e) Latitude at which the peak rate of ITCZ migration occurs. Colors in (d) and (e) indicate runs with mixed layer depths of 10 (black), 5 (red), and 15 m (blue).

to a weaker equivalent potential temperature gradient [cf. (5)], which may reduce the efficacy of temperature feedbacks in these cases. In the case of fast planetary rotation rate, we propose that stronger Coriolis force results in the zonal wind gradient needing to become much steeper to approach angular momentum conservation, and becoming baroclinically unstable at lower latitudes, resulting in a slower transition confined over a smaller range of latitudes. However, we have not been able to conclusively support these ideas, and, as with the transition latitude, a simple explanation of this behavior remains to be determined.

6. The role of eddies

As a final potential control on the rate of movement of the ITCZ, we investigate the role of eddies. Figure 1c shows the seasonal cycle of precipitation and 500-hPa meridional streamfunction for the axisymmetric control-zs simulation. The overall behavior is similar to that of the control simulation (Fig. 1a), with fast shifts from the equinoctial to solstitial state. However, clear differences can also be seen between the eddy-permitting and axisymmetric simulations. The equinoctial state is much shorter-lived in control-zs compared with the control simulation, and the transition occurs more rapidly.

Figure 8 shows the meridional overturning circulation, zonal wind speed, and AM in both the eddy-permitting and axisymmetric experiments for the time periods denoted by the gray bands in Figs. 1a and c. These have been selected such that the first and last bands are over time periods where the control is in the same state as control-zs, while for the middle band the control-zs and control simulations are in the solstitial and equinoctial states, respectively (cf. Fig. 1).

Looking first at the equinoctial state (left column), it can be seen that both simulations have some meridional circulation. However, in control-zs, where there is no eddy driving, this circulation is slightly weaker. We also note that the streamfunction appears to align reasonably well with the AM contours in control-zs compared with in the control. This suggests the flow in this case is close to AM-conserving, as would be expected for a

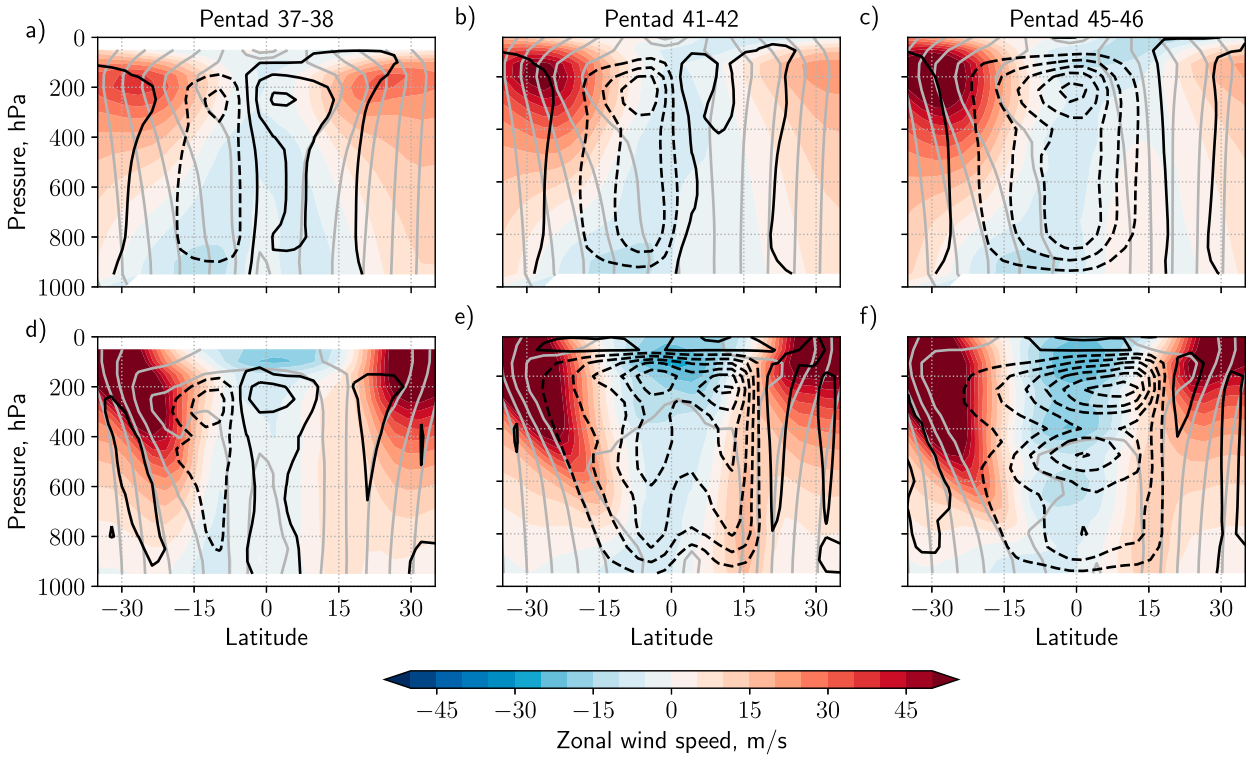

FIG. 8. Zonal wind speed ($\mathrm{m\,s^{-1}}$; colors), mass streamfunction ($\mathrm{kg\,s^{-1}}$; black contours), and AM per unit mass ($\mathrm{m^2\,s^{-1}}$; gray contours) for (a)–(c) the control and (d)–(f) control-zs over the averaging periods indicated in Fig. 1c. For the mass streamfunction, solid contours indicate positive values, and dashed contours indicate negative values, with the zero contour also solid. The contour interval is $100 \times 10^9\,\mathrm{kg\,s^{-1}}$ for the mass streamfunction. For AM, a contour spacing of $\Omega a^2 \cos^2\phi_i$ ($\phi_i = 0°, \pm 5°, \pm 10°, \ldots$) is used, to aid comparison with Bordoni and Schneider (2010).

near-equilibrium, axisymmetric flow [cf. (2)]. The upper-level jets are much stronger in the axisymmetric simulation, but surface winds are weaker. It appears that with no eddies, strong, baroclinically unstable wind and temperature profiles are able to develop, with strong upper-level easterlies at low latitudes, and strong subtropical westerlies.

The middle column of Fig. 8 shows the time period over which the axisymmetric and eddy-permitting simulations are most different. In the control experiment, the winter cell has strengthened slightly relative to the summer cell, but the ITCZ still sits over the equator. In contrast, in the axisymmetric simulation, the ITCZ has shifted into the summer hemisphere, and a strong cross-equatorial circulation has developed. This circulation has a jump at the equator, which Pauluis (2004) showed can occur in an axisymmetric simulation when the temperature gradient is weak. Eventually, both simulations enter the solstitial state. In this state, the Hadley cells in the two experiments have similar strengths, suggesting that eddies do not play the same role in strengthening the circulation as they do in the equinoctial state. The flow in the axisymmetric case appears near-AM-conserving in all time periods. In the later period, the cross-equatorial temperature gradient has strengthened, and the axisymmetric overturning circulation no longer has an equatorial jump.

The upper-level momentum budget, (1), can be expressed in a simplified form to give an equation for v (cf. Bordoni and Schneider 2010):

$$f\overline{v} = M + E + t, \tag{13}$$

where M includes all terms relating to the zonal-mean tendencies, E includes all terms relating to eddies, and t accounts for the time tendency of the zonal wind. Dividing through by the Coriolis parameter, the above can be used to partition the mass streamfunction into components associated with the mean flow Ψ_M, eddies Ψ_E, and time evolution Ψ_t. Figure 9 shows this breakdown for the control and control-zs experiments at 500 hPa. Values are taken at the latitude at which Ψ has its minimum value (i.e., where the Southern Hemisphere cell is strongest), with latitudes south of 7° excluded to eliminate spurious large values introduced by dividing by the Coriolis parameter.

As expected from the discussion in section 1, for the control, we see that throughout winter the Southern Hemisphere Hadley cell has a weak magnitude, and is predominantly eddy driven. In Northern Hemisphere summer this increases in strength rapidly, and is now dominantly in balance with the mean flow, indicating that the cell is now closer to AM-conserving. In the control-zs experiment, where there are no eddies, we instead find that the cell is AM-conserving throughout the year. We therefore note that, although a fast migration of the ITCZ is observed in this simulation, this indicates that no change in the dynamical regime of the cell occurs.

In a seasonally evolving dry model, Bordoni and Schneider (2010) found that eddies sharpened the transition compared with the axisymmetric case. In their simulations, they observed that the overturning circulation in the equinoctial state deviated significantly from an AM-conserving flow. While in their eddy-permitting case, the Coriolis force in the equinoctial regime was balanced by eddy momentum fluxes, in the axisymmetric case they found this was associated with a strong tendency on the zonal wind, indicating a transient equinoctial regime. Dry axisymmetric atmospheres of this kind are known to have equilibration times of around 100 days or more (e.g., Fang and Tung 1999). In contrast, we find that the moist model appears to equilibrate more quickly,[1] with the time tendency Ψ_t negligible in Fig. 9b. Consistent with this, the streamfunction contours in Fig. 8d are generally roughly aligned with the contours of AM, particularly at upper levels. A fast increase in cell strength is still observed as the ITCZ shifts off the equator, possibly relating to the threshold behavior of Plumb and Hou (1992). We note that experiments run with a SST distribution similar to that used in Bordoni and Schneider (2010) gave similar results, with faster ITCZ migrations seen over onset in the axisymmetric case than the eddy permitting case, and that using their diffusion parameterization did not change this behavior (not shown).

The key difference between the results from the moist model presented here, and those from the dry simulations appears to be the equilibration time. Where the equilibration time is slower, the axisymmetric equinoctial regime is a transient state with nonzero overturning circulation. This circulation persists until advective temperature feedbacks cause a transition to the solstitial regime. Here, where the model equilibrates faster, the circulation is AM-conserving throughout the year, and appears to be governed by the threshold behavior discussed in Plumb and Hou (1992) and Emanuel (1995). Transitions are rapid compared with both dry simulations (Bordoni and Schneider 2010), and with the control simulation presented here. From this perspective, the role of eddies is predominantly to allow a stable circulation to exist in the equinoctial state, so that the ITCZ remains near the equator for longer. These results do not preclude an important role for eddies in mediating the regime change in eddy-permitting simulations, and it can be expected that a faster suppression of eddy activity will result in a more rapid transition.

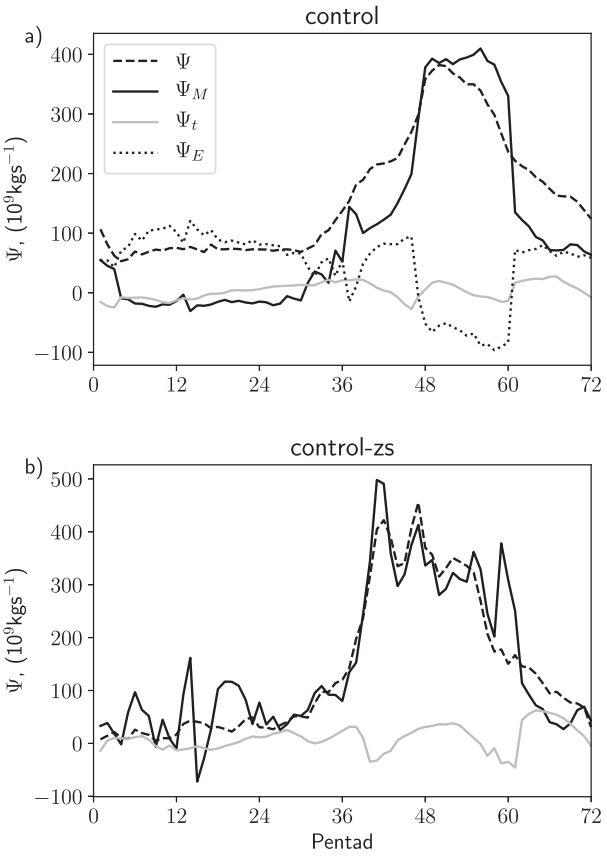

FIG. 9. Breakdown of the 500-hPa overturning strength Ψ into components associated with the zonal-mean flow Ψ_M, eddies Ψ_E, and disequilibrium Ψ_t for (a) the control and (b) control-zs. Values are taken at the latitude at which Ψ takes its minimum value (i.e., where the Southern Hemisphere cell is strongest), but with latitudes south of 7° masked to avoid spurious high values produced by having f on the denominator. Note that values of Ψ here are multiplied by −1 to give positive values for ease of viewing.

[1] Tests indicate that the overturning circulation in the axisymmetric moist model adjusts to an abrupt change in peak SST latitude from 0° to 25°N instantaneously and fully equilibrates within 60 days (not shown).

7. Summary and discussion

Using a range of idealized simulations, we have investigated the controls on the regime changes of the Hadley circulation and consequent shifts of the ITCZ throughout the seasonal cycle. To lowest order, the rate of migration of the ITCZ can be expected to be linearly proportional to the rate of change of the interhemispheric temperature contrast, which, in the absence of changes in the circulation regime, is expected to vary approximately sinusoidally over the annual cycle (Zhou and Xie 2018). By varying the orbital period of an aquaplanet, we have demonstrated that this is indeed the case over much of the year. However, in simulations with a sufficiently shallow mixed layer depth, we find that there is a part of the year, ''aquaplanet monsoon onset,'' over which this linear relation does not apply. At the beginning of the summer season in these experiments, the circulation undergoes a rapid change from an eddy-driven equinoctial regime to an AM-conserving solstitial regime and the ITCZ latitude increases suddenly. This behavior is similar to that seen during the onset of Earth's monsoons. The ITCZ migration rate during this transition does not vary linearly with the orbital period, consistent with the results of previous studies suggesting that dynamical feedbacks are involved in monsoon onset. Interestingly, the peak in the rate of movement of the ITCZ occurs at the same latitude in simulations in which orbital period and mixed layer depth are varied, despite the wide range of climates these changes result in. This suggests that, for a fixed rotation rate, the regime change requires the ITCZ to move a certain distance off of the equator. Consistent with this, in simulations with a deep mixed layer depth or very short orbital period, the ITCZ remains close to the equator and the Hadley circulation does not exhibit any rapid changes, with the circulation unable to leave the equinoctial regime.

The jump in ITCZ latitude in the control simulation is accompanied by a sudden increase in summer-hemisphere surface temperature. Previous work (Schneider and Bordoni 2008) has shown that the temperature tendency due to advection in the lower branch of the Hadley circulation is such as to reinforce the meridional temperature gradient. This results in a positive feedback, strengthening the flow. Our simulated climates are consistent with this. However, in contrast with this previous work, our model also includes a slab ocean, which we find provides an additional feedback onto the circulation via modification of the SST by WISHE. In an experiment in which WISHE is suppressed, we see a second rapid shift of the ITCZ latitude during the transition from the solstitial to equinoctial regime. We find that where WISHE is included, evaporative feedbacks slow this aquaplanet monsoon withdrawal, with low horizontal winds under the ITCZ keeping the evaporative flux from the surface low and maintaining warm SSTs under the ITCZ as it returns to the equator. This evaporative feedback also appears to act to sharpen the transition of the ITCZ off the equator.

While the transition latitude did not vary significantly with orbital period or mixed layer depth, we find that it does vary when the planetary rotation rate is altered. This behavior is consistent with expectations from theories involving the dependence of both the AM-conserving equivalent potential temperature gradient and the momentum/vorticity budgets on planetary rotation rate. Unexpectedly, we also found that when rotation rate is varied, the transition rate varies nonmonotonically with rotation rate. The ITCZ migration rate increases with rotation up to approximately Earth's rotation rate, then decreases, even when the mixed layer depth is also varied. This peak in onset rate near to our rotation rate suggests that Earth may be particularly ''well-tuned'' for a fast monsoon onset. However, a more quantitative exploration of the role of planetary rotation rate in determining both the regime change latitude and rate remains for future work.

Previous studies of monsoon transitions in dry models suggested that eddies are important in sharpening monsoon onset (Bordoni and Schneider 2010). Comparing the control experiment with an axisymmetric simulation forced by the control SSTs, we found that in this moist model, the ITCZ migrations over onset were in fact faster without eddies, and the circulation is AM-conserving throughout the year. This is in contrast with the results from dry models, where a non-AM-conserving equinoctial regime was observed, with the Coriolis force balanced instead by the time tendency of the zonal wind. It appears that with the parameterizations used here, the model equilibrates faster, possibly due to the inclusion of moist processes. The result is a very rapid shift to a cross-equatorial flow once there is thermal forcing off the equator, consistent with Plumb and Hou (1992). This fast transition in our axisymmetric case does not preclude suppression of eddy activity by upper-level easterlies from mediating the transition in eddy-permitting simulations, but it does highlight that an important role of eddies is in allowing an equinoctial circulation to persist for an extended period.

To summarize, in this study we have explored the processes controlling monsoon onset behavior in

aquaplanets. We find that the movement of the ITCZ during the transitions between the equinoctial and solstitial regimes is influenced by thermal feedbacks both internal to the atmosphere and via interactions with the surface via WISHE. Eddies are found to be important in allowing an equinoctial-type regime to persist, but are not essential for sudden changes in ITCZ latitude. The latitude at which the transition occurs varies with planetary rotation rate, but not with mixed layer depth or orbital period, suggesting that planetary parameters play a key role in controlling monsoon onset. If this result can be extended to cases with nonuniform boundary conditions, this insight might prove useful in developing constraints on real-world monsoon behavior.

Open issues remain, including a more quantitative framework for understanding how planetary rotation rate alters the regime change behavior. In future work, we hope to explore this further, and also to extend this framework to the processes involved in cases with nonzonally symmetric boundary conditions, and in particular to understanding Earth's monsoons. In this case, it is expected that land surface processes and land–sea contrast will play more of a role in mediating the regime change, by modifying both the surface and upper-level conditions. In the long term, we hope that additional understanding of the dynamics and feedbacks involved in monsoon onset can help in improving predictability of Asian monsoon onset and in analyzing projections of future changes.

Acknowledgments. The work was supported by the U.K.–China Research and Innovation Partnership Fund, through the Met Office Climate Science for Service Partnership (CSSP) China, as part of the Newton Fund. GKV also acknowledges support from the Royal Society (Wolfson Foundation), the Leverhulme Trust, and NERC Grant NE/M006123/1. The research materials supporting this publication can be accessed by contacting Ruth Geen (rg419@exeter.ac.uk). We thank our three anonymous reviewers for their helpful comments, which greatly improved the final paper.

REFERENCES

Boos, W. R., and K. A. Emanuel, 2008a: Wind-evaporation feedback and abrupt seasonal transitions of weak, axisymmetric Hadley circulations. *J. Atmos. Sci.*, **65**, 2194–2214, https://doi.org/10.1175/2007JAS2608.1.

——, and ——, 2008b: Wind-evaporation feedback and the axisymmetric transition to angular momentum-conserving Hadley flow. *J. Atmos. Sci.*, **65**, 3758–3778, https://doi.org/10.1175/2008JAS2791.1.

Bordoni, S., and T. Schneider, 2008: Monsoons as eddy-mediated regime transitions of the tropical overturning circulation. *Nat. Geosci.*, **1**, 515–519, https://doi.org/10.1038/ngeo248.

——, and ——, 2010: Regime transitions of steady and time-dependent Hadley circulations: Comparison of axisymmetric and eddy-permitting simulations. *J. Atmos. Sci.*, **67**, 1643–1654, https://doi.org/10.1175/2009JAS3294.1.

Caballero, R., R. T. Pierrehumbert, and J. L. Mitchell, 2008: Axisymmetric, nearly inviscid circulations in non-condensing radiative-convective atmospheres. *Quart. J. Roy. Meteor. Soc.*, **134**, 1269–1285, https://doi.org/10.1002/qj.271.

Clough, S. A., M. W. Shephard, E. J. Mlawer, J. S. Delamere, M. J. Iacono, K. Cady-Pereira, S. Boukabara, and P. D. Brown, 2005: Atmospheric radiative transfer modeling: A summary of the AER codes. *J. Quant. Spectrosc. Radiat. Transf.*, **91**, 233–244, https://doi.org/10.1016/j.jqsrt.2004.05.058.

Donohoe, A., J. Marshall, D. Ferreira, and D. Mcgee, 2013: The relationship between ITCZ location and cross-equatorial atmospheric heat transport: From the seasonal cycle to the Last Glacial Maximum. *J. Climate*, **26**, 3597–3618, https://doi.org/10.1175/JCLI-D-12-00467.1.

Emanuel, K. A., 1995: On thermally direct circulations in moist atmospheres. *J. Atmos. Sci.*, **52**, 1529–1534, https://doi.org/10.1175/1520-0469(1995)052<1529:OTDCIM>2.0.CO;2.

Fang, M., and K. K. Tung, 1999: Time-dependent nonlinear Hadley circulation. *J. Atmos. Sci.*, **56**, 1797–1807, https://doi.org/10.1175/1520-0469(1999)056<1797:TDNHC>2.0.CO;2.

Faulk, S., J. Mitchell, and S. Bordoni, 2017: Effects of rotation rate and seasonal forcing on the ITCZ Extent in planetary atmospheres. *J. Atmos. Sci.*, **74**, 665–678, https://doi.org/10.1175/JAS-D-16-0014.1.

Frierson, D. M. W., 2007: The dynamics of idealized convection schemes and their effect on the zonally averaged tropical circulation. *J. Atmos. Sci.*, **64**, 1959–1976, https://doi.org/10.1175/JAS3935.1.

——, and Y. T. Hwang, 2012: Extratropical influence on ITCZ shifts in slab ocean simulations of global warming. *J. Climate*, **25**, 720–733, https://doi.org/10.1175/JCLI-D-11-00116.1.

——, I. M. Held, and P. Zurita-Gotor, 2006: A gray-radiation aquaplanet moist GCM. Part I: Static stability and eddy scale. *J. Atmos. Sci.*, **63**, 2548–2566, https://doi.org/10.1175/JAS3753.1.

Geen, R., F. H. Lambert, and G. K. Vallis, 2018: Regime change behavior during Asian monsoon onset. *J. Climate*, **31**, 3327–3348, https://doi.org/10.1175/JCLI-D-17-0118.1.

Jucker, M., and E. P. Gerber, 2017: Untangling the annual cycle of the tropical tropopause layer with an idealized moist model. *J. Climate*, **30**, 7339–7358, https://doi.org/10.1175/JCLI-D-17-0127.1.

Kim, H.-k., and S. Lee, 2001: Hadley Cell dynamics in a primitive equation model. Part II: Nonaxisymmetric flow. *J. Atmos. Sci.*, **58**, 2859–2871, https://doi.org/10.1175/1520-0469(2001)058<2859:HCDIAP>2.0.CO;2.

Lindzen, R. S., and A. Y. Hou, 1988: Hadley circulations for zonally averaged heating centered off the equator. *J. Atmos. Sci.*, **45**, 2416–2427, https://doi.org/10.1175/1520-0469(1988)045<2416:HCFZAH>2.0.CO;2.

Mlawer, E. J., S. J. Taubman, P. D. Brown, M. J. Iacono, and S. A. Clough, 1997: Radiative transfer for inhomogeneous atmospheres: RRTM, a validated correlated-k model for the longwave. *J. Geophys. Res.*, **102**, 16 663–16 682, https://doi.org/10.1029/97JD00237.

O'Gorman, P. A., and T. Schneider, 2008: The hydrological cycle over a wide range of climates simulated with an

idealized GCM. *J. Climate*, **21**, 3815–3832, https://doi.org/10.1175/2007JCLI2065.1.

Pauluis, O., 2004: Boundary layer dynamics and cross-equatorial Hadley circulation. *J. Atmos. Sci.*, **61**, 1161–1173, https://doi.org/10.1175/1520-0469(2004)061<1161:BLDACH>2.0.CO;2.

Plumb, R. A., and A. Y. Hou, 1992: The response of a zonally symmetric atmosphere to subtropical thermal forcing: Threshold behavior. *J. Atmos. Sci.*, **49**, 1790–1799, https://doi.org/10.1175/1520-0469(1992)049<1790:TROAZS>2.0.CO;2.

Privé, N. C., and R. A. Plumb, 2007: Monsoon dynamics with interactive forcing. Part II: Impact of eddies and asymmetric geometries. *J. Atmos. Sci.*, **64**, 1431–1442, https://doi.org/10.1175/JAS3917.1.

Satoh, M., 1994: Hadley circulations in radiative-convective equilibrium in an axially symmetric atmosphere. *J. Atmos. Sci.*, **51**, 1947–1968, https://doi.org/10.1175/1520-0469(1994)051<1947:HCIREI>2.0.CO;2.

Schneider, E. K., 1984: Response of the annual and zonal mean winds and temperatures to variations in the heat and momentum sources. *J. Atmos. Sci.*, **41**, 1093–1115, https://doi.org/10.1175/1520-0469(1984)041<1093:ROTAAZ>2.0.CO;2.

Schneider, T., and S. Bordoni, 2008: Eddy-mediated regime transitions in the seasonal cycle of a Hadley circulation and implications for monsoon dynamics. *J. Atmos. Sci.*, **65**, 915–934, https://doi.org/10.1175/2007JAS2415.1.

Shaw, T. A., 2014: On the role of planetary-scale waves in the abrupt seasonal transition of the Northern Hemisphere general circulation. *J. Atmos. Sci.*, **71**, 1724–1746, https://doi.org/10.1175/JAS-D-13-0137.1.

Vallis, G., and Coauthors, 2018: Isca, v1.0: A framework for the global modelling of the atmospheres of Earth and other planets at varying levels of complexity. *Geosci. Model Dev.*, **11**, 843–859, https://doi.org/10.5194/gmd-11-843-2018.

Walker, J. M., and S. Bordoni, 2016: Onset and withdrawal of the large-scale South Asian monsoon: A dynamical definition using change point detection. *Geophys. Res. Lett.*, **43**, 11 815–11 822, https://doi.org/10.1002/2016GL071026.

Wilks, D. S., 2011: *Statistical Methods in the Atmospheric Sciences*. 3rd ed. International Geophysics Series, Vol. 100, Academic Press, 704 pp.

Xie, S. P., and N. Saiki, 1999: Abrupt onset and slow seasonal evolution of summer monsoon in an idealized GCM simulation. *J. Meteor. Soc. Japan*, **77**, 949–968, https://doi.org/10.2151/jmsj1965.77.4_949.

Yin, M. T., 1949: Synoptic-aerologic study of the onset of the summer monsoon over India and Burma. *J. Meteor.*, **6**, 393–400, https://doi.org/10.1175/1520-0469(1949)006<0393:SASOTO>2.0.CO;2.

Zhou, W., and S. P. Xie, 2018: A hierarchy of idealized monsoons in an intermediate GCM. *J. Climate*, **31**, 9021–9036, https://doi.org/10.1175/JCLI-D-18-0084.1.